Superparamagnetic Aluminosilicates

Mesoporous Aluminosilicate Materials with Superparamagnetic γ-Fe_2O_3 Particles Embedded in the Walls**

*Carlos Garcia, Yuanming Zhang, Francis DiSalvo, and Ulrich Wiesner**

Silica-based mesostructured and mesoporous materials have sparked much interest among researchers over the last decade[1–5] expanding their functionality by the incorporation of functional organic compounds,[6–8] substitution or addition of other inorganic materials,[9] or templating into carbon-based materials.[10] Here we will focus on magnetic mesoporous materials. Although research has been performed on surfactant-based templating and sonochemical approaches to layered iron oxide/oxyhydroxide mesophases,[11,12] polymer-derived magnetic bulk ceramics,[13] and bulk iron oxide silicates prepared through sol–gel techniques,[14–17] research on mesostructured iron-containing silicates is scarce and limited to surfactant-based systems where the iron compound was loaded after synthesis.[18,19] Backfilling the pores is a common technique to functionalize mesoporous materials,[20] but it requires more synthesis and characterization steps and, more importantly, risks clogging the pore structure. We present a simple block-copolymer-based "one-pot" self-assembly approach to multifunctional γ-iron oxide aluminosilicates that are mesoporous and exhibit superparamagnetic behavior. Nanoscopic iron oxide particles are incorporated in the walls of the aluminosilicate matrix. Therefore, the blocking of the pores, as observed in earlier studies on backfilled materials, is overcome, even for high iron loadings.[19] We anticipate that this simple and versatile block-copolymer-directed approach to large-pore structures will lead to new techniques for the separation of magnetically labeled biological macromolecules that combine size exclusion as well as magnetic interactions. Also, the robust matrix has thick walls (>10 nm) which give the material good thermal stability (as high as 800 °C) allowing for catalytic applications at elevated temperatures.

The synthesis is unique in allowing for precise control over the structure and composition of the final materials. Although only the inverse-hexagonal cylinder morphology is described (cylindrical pores in a aluminosilicate matrix), several morphologies were observed in our laboratories, similar to those seen for diblock copolymers and their mixtures with homopolymers.[21,22] These morphologies include the hexagonal cylinder (inorganic cylinders in a polymer matrix) and the lamellar phases. The approach can also be extended to other transition-metal oxide systems. Iron oxide was used in our study for its potential magnetic properties, but also serves as an example of what should be possible from a wide range of commercially available metal alkoxides. The actual composition of the resulting materials can be tailored according to the application, which becomes particularly important in catalyst technology.

The amphiphilic diblock copolymer, poly(isoprene-*block*-ethylene oxide) (PI-*b*-PEO), served as a structure-directing agent. Two polymers of different molecular weight and PEO fraction were used (P5: $M_W = 22\,400$, 15 wt % PEO; P7: $M_W = 38\,600$, 32 wt % PEO). The polymers had a low molecular-weight distribution with a polydispersity index of less than 1.05. A sol was prepared using (3-glycidoxypropyl)trimethoxysilane (Sigma–Aldrich) and aluminum-*sec*-butoxide (Sigma–Aldrich), which was mixed with a solution of the polymer and iron(III) ethoxide powder (Gelest, Inc.) to prepare polymer–inorganic composites with 25 mol % Fe, based on the cation. The ratio of inorganic material to polymer was 2.37 for the composite made with P5 (designated as C5) and 2.25 for the composite made with P7 (designated

[*] Prof. Dr. U. Wiesner, C. Garcia, Y. Zhang
Department of Materials Science and Engineering
Cornell University
329 Bard Hall, Ithaca, NY 14853 (USA)
Fax: (+1) 607-255-2365
E-mail: ubw1@cornell.edu
Prof. Dr. F. DiSalvo
Department of Chemistry and Chemical Biology
Cornell University
Baker Laboratory, Ithaca, NY 14853-2501 (USA)

[**] This work was supported by the National Science Foundation (DMR-0072009), Philip Morris, and the Cornell Center for Materials Research (CCMR), a Materials Research Science and Engineering Center of the National Science Foundation (DMR-0079992). In particular, we thank Malcolm Thomas in the CCMR UHV-STEM laboratory for support as well as the CCMR X-Ray Diffraction Facility, the CCMR Hudson Mesoscale Processing Facility, and the Electron and Optical Microscopy Facility. We thank Yuri Suzuki and Bruce Van Dover for the use of the SQUID magnetometer and fruitful discussions of the magnetic data.

 © 2003 Wiley-VCH Verlag GmbH & Co. KGaA, Weinheim DOI: 10.1002/ange.200250618

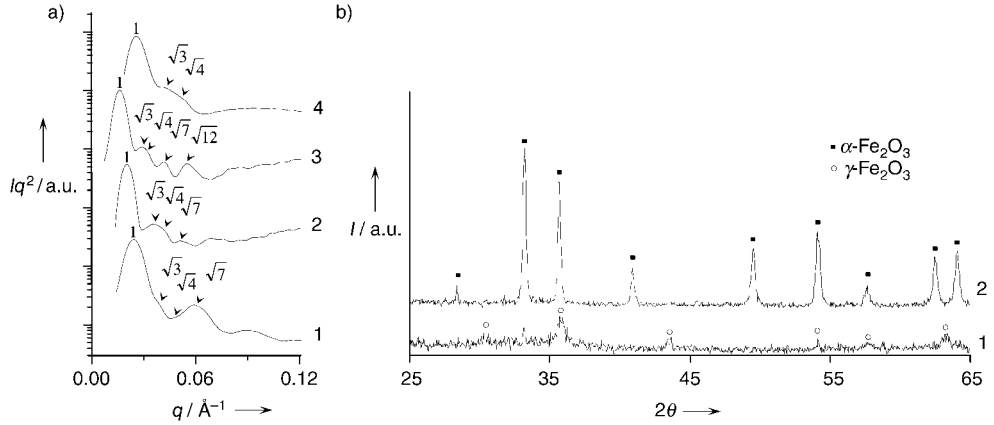

Figure 1. a) SAXS analysis of the pure block-copolymer P7 (trace 1), the as-prepared 25 mol% Fe-containing polymer–inorganic composites C5 and C7 (traces 2 and 3, respectively), and C7 calcined to 750°C (trace 4). Positions of the higher order peaks suggest a hexagonal structure in all cases; b) XRD analysis of the bulk ceramics (prepared without block copolymer) calcined to 550°C. Pure $Fe(OH)_3$ and 50 mol% Fe-containing aluminosilicate (diffractograms 1 and 2, respectively) prepared using the same sol–gel synthesis procedure as for the composites. Symbols indicate expected peaks from α-Fe_2O_3 (■) and γ-Fe_2O_3 (○), respectively. SAXS experiments were performed on a Bruker-AXS Nanostar diffractometer ($Cu_{K\alpha}$, 1.54 Å) operated at 40 kV, 40 mA in transmission. Data were recorded using a 2D Hi-Star aerial detector with a sample to detector distance of 62.5 cm. Integration of the images was performed over all azimuthal angles and resulting profiles smoothed using an FFT filter. XRD data was obtained from powdered samples using a Scintag Inc. θ–θ diffractometer ($Cu_{K\alpha}$, 1.54 Å).

as C7). This ratio was based on the amount of inorganic material remaining after evaporation of all the volatile components (experimentally found to be 55% of initial weight of the sol).

Figure 1a shows small-angle X-ray scattering (SAXS) data for the pure diblock copolymer P7 and the two as-prepared polymer–inorganic composites C5 and C7 (traces 1–3, respectively). The scattering data exhibit higher order peaks for both the polymer and the composites, indicative of cylinders in a hexagonal array. Transmission electron microscopy (TEM) corroborates these assignments. Figure 2 depicts representative TEM micrographs of the as-prepared composite C5 (Figure 2a,b) showing a well-defined inverse-hexagonal morphology. The absence of large-angle X-ray diffraction (XRD) peaks (data not shown) demonstrates that the inorganic and polymer components of the composites are amorphous.

For the production of a crystalline magnetic iron oxide phase, the as-prepared composites were calcined at elevated temperatures in air. To elucidate the effect of our aluminosilicate matrix on the iron oxide formation, XRD experiments were performed on two test samples made from only the inorganic precursors (that is, without block copolymer) and heated to 550°C in air. The results of these measurements are shown in Figure 1b. The first sample was made by heating fully hydrolyzed iron ethoxide, and was shown to be crystalline non-magnetic α-Fe_2O_3 (Figure 1b, upper diffractogram). The second sample was made from an iron-containing aluminosilicate (50 mol% Fe) and showed a poorly crystalline γ-Fe_2O_3 phase (Figure 1b, lower diffractogram). These results on model materials suggest that in a bulk aluminosilicate matrix, γ-Fe_2O_3 is the only detected crystalline phase after heat treatment at elevated temperatures (550°C). It should be noted that comparable results, that is, the formation of only γ-Fe_2O_3 in iron-containing silicate materials prepared by similar means, were also obtained by other groups.[14–17,23] Although pure γ-Fe_2O_3 usually decomposes to nonmagnetic α-Fe_2O_3 at approximately 350°C, the remaining amorphous aluminosilicate matrix apparently hinders the transformation, thus stabilizing the γ-phase, even when heated to 750°C.[17] This is fortunate since one can now exploit the magnetic behavior of γ-Fe_2O_3.

Small-angle X-ray data for composite C7 after calcination at 750°C is shown in Figure 1a (trace 4). Compared to the as-prepared material (Figure 1a, trace 3) the diffractogram is shifted to significantly higher q values, as expected from the considerable weight loss (approximately 70%, as given by thermogravimetric analysis) during heat treatment.[21,24] This weight loss results from the oxidation of all organic constituents to volatile products. The diffractogram clearly shows higher order reflections suggesting that the mesoscopic order has been preserved. Assuming retention of the hexagonal structure, the (10) interplane distance after calcination at 750°C was reduced by 36% from the as-prepared composite owing to the shrinkage of the matrix. XRD experiments on this material did not generate any identifiable diffraction peaks from iron oxide particles. This is most likely because of the small size of the iron oxide crystallite domains (see below).

The magnetic properties of C7 before and after calcination at different temperatures were investigated using a SQUID magnetometer (Figure 3). As expected, the magnetization of the as-prepared composite exhibits paramagnetic behavior. However, after calcination at 550°C, the onset of an inflection point and the absence of residual magnetization at zero applied field in the field (H) versus magnetization (M) plot indicates superparamagnetic behavior. As the calcination temperatures were increased above 550°C, the measured magnetization also increased. At the same time, the sigmoidal nature of the superparamagnetic response became more

 © 2003 Wiley-VCH Verlag GmbH & Co. KGaA, Weinheim

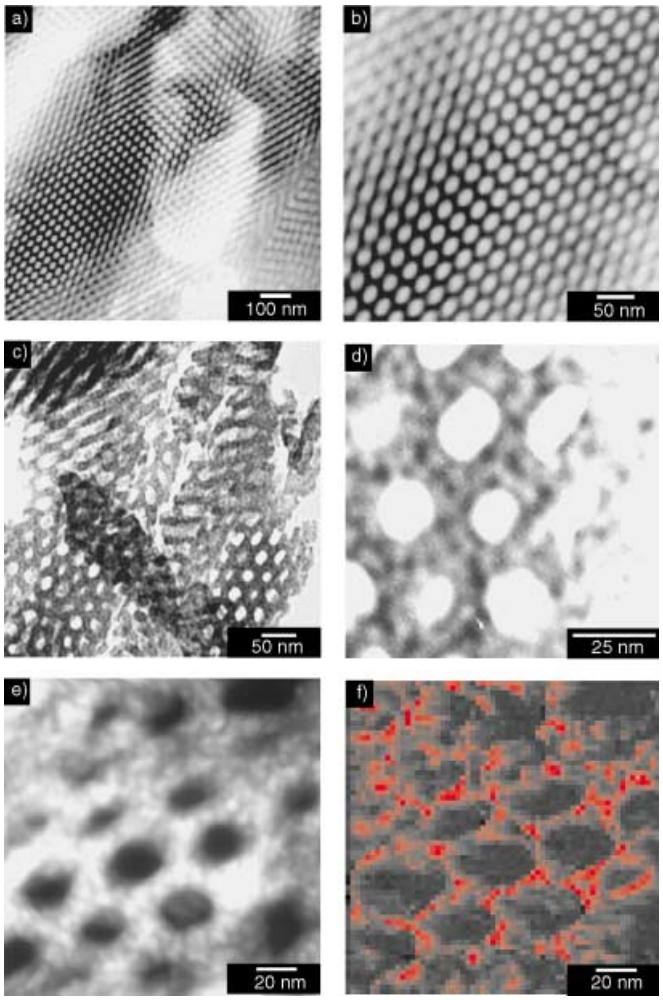

Figure 2. a,b) Bright-field TEM images of the as-made C5 sample at two different magnifications revealing the inverse-hexagonal morphology; c,d) bright-field TEM images of C7 after calcination to 750 °C at two different magnifications. Hexagonal order is shown (c) to be preserved after calcination, while at higher magnification (d), the iron oxide precipitates show up as dark spots within the matrix of the inverse-hexagonal morphology; e,f) annular dark-field STEM images of C7 calcined to 750 °C (e), together with the corresponding energy-filtered iron distribution map (f). Samples were cut into ultrathin sections with a Leica Ultracut UCT microtome at 300 K. Bright-field TEM micrographs were taken on a Jeol 1200EX operating at 120 kV. A VG HB-501UX dedicated STEM was used to acquire images e) and f) operating at 100 keV with a cold field emission source to produce high-resolution bright-field (resolution ~0.3 nm) and annular dark-field (resolution ~0.2 nm) images. A single-crystal YAP scintillator/PMT combination was used for serial EELS and energy-filtered imaging with resolution of less than 1 eV obtained in the 0–2 keV range.

apparent, and was most developed for the composite calcined at 750 °C. The magnetic response of the ceramic material suggests the nucleation and growth of small γ-Fe_2O_3 particles.

To quantitatively determine the iron oxide precipitate size, zero-field-cooling (ZFC) and field-cooling (FC) experiments were performed on C7 calcined to 750 °C. The data in the inset of Figure 3 indicates a blocking temperature of 25 K and a collapse temperature (the temperature where the two curves deviate from each other) of 35 K. Both the narrowness of the ZFC curve around the maximum and the low collapse temperature are strong indications of a narrow size distribution of the particles within the matrix.[25] According to superparamagnetic theory,[26] the particle volume can be determined from the blocking temperature based on the Arrhenius relationship:

$$\tau_m = \tau_0 \exp\left(\frac{K V}{k_B T_B}\right) \quad (1)$$

where τ_m is the experimental measurement time (100 s for the SQUID magnetometer), τ_0 is a time constant characteristic to the material, K is the anisotropy constant, V is the volume of the magnetic particle, k_B is the Boltzmann constant, and T_B is the blocking temperature. Detailed analysis of the magnetic properties of small magnetic domains based on γ-Fe_2O_3 have been performed by several research groups.[15,25,27] From these studies, the anisotropy constant K was estimated to be $1 \times 10^5\ J\,m^{-3}$ and τ_0 to be 10^{-10} s, which results in a calculated average γ-Fe_2O_3 particle size of 5.6 nm. Fitting the magnetization curve (M versus H) of sample C7 (750 °C calcination) at 60 K, that is, 35 K above T_B, to the Langevin function from the classical theory of paramagnetism indicates approximately 350 spins per particle.[28]

To corroborate the scattering and SQUID results, TEM was performed on C7 calcined to 750 °C. The TEM micrograph in Figure 2c demonstrates that upon calcination the inverse-hexagonal morphology of the material is preserved, as suggested by the SAXS data in Figure 1. From the TEM micrograph the (10) interplane distance was measured to be 25 nm, which is in good agreement with the value of 24.5 nm calculated from SAXS. Furthermore, the higher resolution image in Figure 2d shows homogeneously distributed dark spots within the matrix. A histogram of the size distribution of these precipitates reveals an average particle diameter of approximately 5 nm. Considering that TEM is a local technique, this number is in excellent agreement with the calculated γ-Fe_2O_3 particle size of 5.6 nm determined by the SQUID data, which represents measurements integrated over macroscopic sample dimensions. This remarkable result indicates that the particle-size distribution reflected from the TEM micrograph in Figure 2d is representative of the entire sample, and suggests the amazing structural control of the present approach. To directly show that these precipitates contain iron, we performed elemental mapping on a scanning transmission electron microscope (STEM) using electron energy loss spectroscopy (EELS).[29] The dark-field image of C7 calcined to 750 °C and the corresponding elemental iron map are shown in Figure 2e and f, respectively. Iron is clearly abundant and clustered together, which is consistent with iron oxide precipitates.

These data demonstrate that, first, a ceramic with ordered mesoscale pores is obtained upon calcination to temperatures as high as 750 °C and, secondly, that nucleation and growth of γ-Fe_2O_3 precipitates occurs inside the amorphous aluminosilicate matrix walls. This latter result is consistent with the phase separation of Fe_2O_3 and SiO_2 observed in their bulk phase diagram.[30] The result is a mesoporous material with open and accessible pores and superparamagnetic properties.

 © 2003 Wiley-VCH Verlag GmbH & Co. KGaA, Weinheim

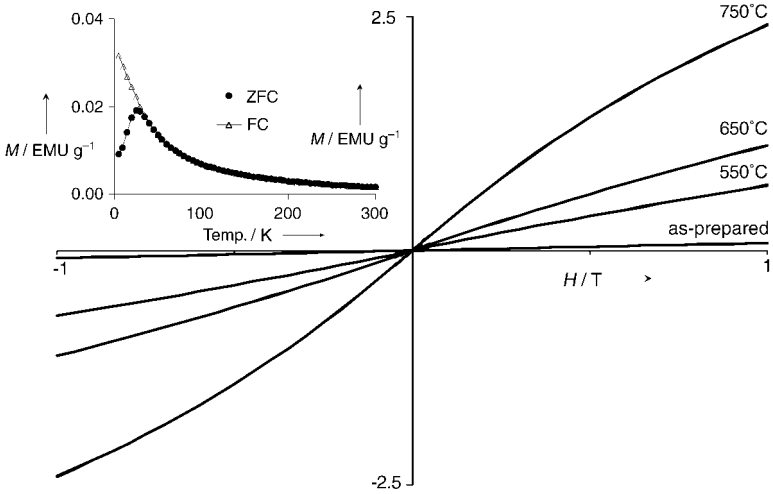

Figure 3. Field dependence of the magnetic properties of C7, both as-prepared and calcined to different temperatures, as indicated in the figure. Inset: zero-field cooling (ZFC) and field cooling (FC) curves for sample P7-C25 calcined to 750 °C. Data were collected on a Quantum Design MPMS SQUID magnetometer at 300 K for the *H* versus *M* curves and a 200 Oe field was used for the ZFC/FC experiments.

Indeed, the calcined materials exhibit a nitrogen sorption isotherm of type IV according to BDDT classification, with a specific surface area of 310 m^2g^{-1} according to the Brunnauer–Emmett–Teller (BET) method, and a pore-size distribution with an average pore diameter according to Barrett–Joyner–Halenda (BJH) of 8.3 nm (data not shown).[31,32] These values are in excellent agreement with measurements on similar PI-*b*-PEO block-copolymer-derived mesoporous aluminosilicate materials prepared without the addition of iron and show that the present self-assembly approach does not lead to clogging of the pore structure,[21] even for significant iron loadings. In contrast, previous studies on mesoporous materials backfilled with iron oxide in a post-synthesis step showed significant pore clogging with as little as 6 wt % iron incorporation.[19] It is interesting to note from the TEM micrograph in Figure 2 d that the iron oxide precipitates extend to the surface of the pores in the mesoporous aluminosilicate matrix. For applications in catalysis this is a particularly important feature and originates from the present one-pot synthesis without additional synthesis steps. Furthermore, with the wall thickness easily exceeding 10 nm, the materials are unusually stable to high temperatures.

Completely novel applications can also be envisioned for such multifunctional materials, for example, the separation of magnetically labeled biomolecules. In the presence of an external magnetic field, diffusion of these labeled molecules through the pores would be retarded through multiple interactions with the fringe magnetic fields of the γ-Fe_2O_3 at the pore surfaces. After unlabeled material passes through, the magnetic field could be switched off to release the labeled molecules from the medium, thus leading to efficient separation of labeled and unlabeled species. The present materials have not been optimized for any of these applications, but clearly engineering the pore and precipitate sizes, as well as particle distribution towards these goals, is now possible.

In this paper we have presented a simple block-copolymer-based one-pot self-assembly approach to superparamagnetic mesoporous materials with large pores, thick walls, and well-defined magnetic iron oxide particles within the walls of the matrix. Blocking of the pores as observed in earlier studies on backfilled materials is thus overcome, even for high iron loadings. The multifunctional nanostructured materials open up access to novel biopolymer separation technologies combining size-exclusion principles with separation of magnetically labeled materials. Furthermore, they should enable potential catalytic applications at elevated temperatures.

Experimental Section

Each polymer was dissolved in a dry THF/chloroform mixture (1:1 w/w) to form a 5 wt % solution. Iron(III) ethoxide powder (Gelest, Inc.) was added to this solution in the desired amounts. A separate solution of (3-glycidoxypropyl)trimethoxysilane (GLYMO) and aluminum-*sec*-butoxide (9:1 molar ratio) was prepared following a two-step acid-catalyzed hydrolysis procedure described previously.[4] Potassium chloride was added (0.3 wt %) to shield surface charges for improved cross-linking of the sol. This sol was then added in varying amounts to the polymer–iron(III) ethoxide solution and stirred for one hour. It is important to note that the iron ethoxide was not added to the aluminosilicate sol–gel precursor solution since the rapid hydrolysis and condensation kinetics of this compound in the presence of water and an acid catalyst leads to premature precipitation of an iron oxide phase. Films were cast by evaporation of the solvents and byproducts on a hotplate at 50 °C and then at 130 °C in a vacuum oven for one hour.

Heat treatment was performed in a tube furnace under aerobic conditions by ramping up the temperature in 1 °C min^{-1} increments to the final calcination temperatures. Each ramp was held at 350 °C for three hours and then for another six hours at the final calcination temperature.

Received: November 25, 2002 [Z50618]

Keywords: block copolymers · iron · magnetic properties · mesoporous materials · oxides

[1] C. T. Kresge, M. E. Leonowicz, W. J. Roth, J. C. Vartuli, J. S. Beck, *Nature* **1992**, *359*, 710.
[2] G. S. Attard, J. C. Glyde, C. G. Göltner, *Nature* **1995**, *378*, 366.
[3] S. A. Bagshaw, E. Prouzet, T. J. Pinnavaia, *Science* **1995**, *269*, 1242.
[4] M. Templin, A. Franck, A. Du Chesne, H. Leist, Y. Zhang, R. Ulrich, V. Schädler, U. Wiesner, *Science* **1997**, *278*, 1795.
[5] D. Zhao, J. Feng, Q. Huo, N. Melosh, G. H. Fredrickson, B. F. Chmelka, G. D. Stucky, *Science* **1998**, *279*, 548.
[6] Y. Lu, Y. Yang, A. Sellinger, M. Lu, J. Huang, H. Fan, R. Haddad, G. Lopez, A. R. Burns, D. Y. Sasaki, J. Shelnutt, C. J. Brinker, *Nature* **2001**, *410*, 913.
[7] T. Asefa, M. J. MacLachlan, N. Coombs, G. A. Ozin, *Nature* **1999**, *402*, 867.
[8] S. Inagaki, S. Guan, T. Ohsuna, O. Terasaki, *Nature* **2002**, *416*, 304.

 © 2003 Wiley-VCH Verlag GmbH & Co. KGaA, Weinheim

[9] P. Yang, D. Zhao, D. I. Margolese, B. F. Chmelka, G. D. Stucky, *Nature* **1998**, *396*, 152.
[10] S. H. Joo, S. J. Choi, I. Oh, J. Kwak, Z. Liu, O. Terasaki, R. Ryoo, *Nature* **2001**, *412*, 169.
[11] G. Wirnsberger, K. Gatterer, H. P. Fritzer, W. Grogger, P. Behrens, M. F. Hansen, C. B. Koch, *Chem. Mater.* **2001**, *13*, 1153.
[12] Y. Wang, L. Yin, A. Gedanken, *Ultrason. Sonochem.* **2002**, *9*, 285.
[13] M. J. MacLachlan, G. Madlen, N. Coombs, T. W. Coyle, N. P. Raju, J. E. Greedan, G. A. Ozin, I. Manners, *Science* **2000**, *287*, 1460.
[14] F. del Monte, M. P. Morales, D. Levy, A. Fernandez, M. Ocana, A. Roig, E. Molins, K. O'Grady, C. J. Serna, *Langmuir* **1997**, *13*, 3627.
[15] G. Ennas, A. Musinu, G. Piccaluga, D. Zedda, D. Gatteschi, C. Sangregorio, J. L. Stanger, G. Concas, G. Spano, *Chem. Mater.* **1998**, *10*, 495.
[16] C. Cannas, M. F. Casula, G. Concas, A. Corrias, D. Gatteschi, A. Falqui, A. Musinu, C. Sangregorioc, G. Spanob, *J. Mater. Chem.* **2001**, *11*, 3180.
[17] M. F. Casula, A. Corrias, G. Paschina, *J. Non-Cryst. Solids* **2001**, *293–295*, 25.
[18] M. Fröba, R. Köhn, G. Bouffaud, O. Richard, G. van Tendeloo, *Chem. Mater.* **1999**, *11*, 2858.
[19] L. Zhang, G. C. Papaefthymiou, J. Y. Ying, *J. Phys. Chem. B* **2001**, *105*, 7414.
[20] X. He, D. Antonelli, *Angew. Chem.* **2002**, *114*, 222; *Angew. Chem. Int. Ed.* **2002**, *41*, 214.
[21] P. F. W. Simon, R. Ulrich, H. W. Spiess, U. Wiesner, *Chem. Mater.* **2001**, *13*, 3464.
[22] I. W. Hamley, *The Physics of Block Copolymers*, Oxford University Press. Oxford, **1998**.
[23] D. Niznansky, N. Viart, J. L. Rehspringer, *J. Sol-Gel Sci. Technol.* **1997**, *8*, 615.
[24] A. C. Finnefrock, R. Ulrich, A. Du Chesne, C. C. Honeker, K. Schumacher, K. K. Unger, S. M. Gruner, U. Wiesner, *Angew. Chem.* **2001**, *113*, 1247; *Angew. Chem. Int. Ed.* **2001**, *40*, 1208.
[25] B. H. Sohn, R. E. Cohen, G. C. Papaefthymiou, *J. Magn. Magn. Mater.* **1998**, *182*, 216.
[26] A. Aharoni, *Relaxation Processes in Small Particles*, North Holland, Amsterdam, **1992**.
[27] C. Djega-Mariadassou, J. L. Dormann, M. Nogués, G. Villers, S. Sayouri, *IEEE Trans. Magn.* **1990**, *26*, 1819.
[28] B. D. Cullity, *Introduction to Magnetic Materials*, Addison-Wesley, Reading, MA, **1972**.
[29] M. M. Disko, *Transmission Electron Energy Loss Spectroscopy in Materials Science, Vol. 2*, The Minerals, Metals and Materials Society, Pennsylvania, **1992**.
[30] *Phase Diagrams for Ceramists, Vol. 1*, American Ceramic Society, Columbus, OH, **1985**.
[31] E. P. Barrett, L. G. Joyner, P. P. Halenda, *J. Am. Chem. Soc.* **1951**, *73*, 373.
[32] S. Brunauer, L. S. Deming, W. S. Deming, E. Teller, *J. Am. Chem. Soc.* **1940**, *62*, 1723.

 © 2003 Wiley-VCH Verlag GmbH & Co. KGaA, Weinheim